
Combined Uses of Supervised Classification and Normalized Difference Vegetation Index Techniques to Monitor Land Degradation in the Saloum Saline Estuary System

Ndeye Maguette Dieng, Joel Dinis, Serigne Faye, Marçia Gonçalves, and Mário Caetano

Abstract

Saltwater contamination constitutes a serious problem in Saloum estuary, due to the intermittent and reverse tide flows of the Saloum River. This phenomenon is caused by the runoff deficit, which forces the advance of saltwater 60 km upstream, contaminating surface water and thus causing the degradation of biodiversity and large areas of agricultural soils in this region. The present study aims to evaluate the consequences of saltwater contamination in the last three decades in this estuary by assessing the land-cover dynamics. Thus, latter consists of tracking the landscape-changing process over time to identify land-cover transitions. These transitions are closely related to the ecosystem-setting condition and can be used to assess the combined impacts of both natural and human-induced phenomena over a given period of time. In this study, special attention was given to mangrove degradation and to temporal progression of the salty barren soils locally called “tan”. The loss of mangrove areas to tan and the general increase in salty barren soil areas can reflect the increase in the level of salinization in the study area over the time period under consideration. To fulfill this objective, four Landsat satellite images from the same season in the years 1984, 1992, 1999, and 2010 were used to infer time series land-use and land-cover maps of the Saloum estuary area. In addition to satellite imagery, rainfall records were used to evaluate climatic variation in terms of high-to-low precipitation during the time span considered. Spectral analysis indicated that from 1984 to 2010, mangroves and savanna/rain-fed agriculture are converted to “tan” (denuded and salty soils). In addition, these results showed that significant changes in land use/land cover occur within the whole estuary system and reflecting therefore environmental degradation, such as land desertification and salinization, and vegetation degradation which reflect the advanced of salinity.

N. M. Dieng (✉) · S. Faye
Geology Department, Faculty of Sciences and Techniques
University Cheikh Anta Diop, P.O. Box 5005, Dakar, Senegal
e-mail: diengmaguette@yahoo.fr; ndeye81.dieng@ucad.edu.sn

S. Faye
e-mail: fayerigrignel@gmail.com

J. Dinis · M. Caetano
Higher Institute of Statistics and Information Management,
New University of Lisbon, Lisbon, Portugal

M. Gonçalves
Remote Sensing Unit of the Portuguese Geographic Institute,
Lisbon, Portugal

Keywords

Saloum inverse estuary • Salinization • Normalized difference vegetation index • Mangrove degradation • Change detection • Inverse estuary

Introduction

Evidence is mounting that we are in a period of climate changes brought about by increasing atmospheric concentrations of greenhouse gases. Due to increases in global temperature, sea level may rise from 0.5 m to more than 1.0 m above current mean sea level by the year 2100 (Church and White 2006; Overpeck et al. 2006; IPCC 2007). It is even expected that temperature rise over the next century would probably be greater than that observed in the last 10,000 years. As a direct consequence of warming temperature, the hydrologic cycle will undergo significant impact with accompanying changes in the rates of precipitation and evaporation. Predictions include higher incidences of severe weather events, a higher likelihood of flooding, and more droughts. Sea level rise as a result of global warming has an impact on the increasing inundation on coastal area.

In addition to these impacts, the economic, social, and environmental consequences will be enormous in Africa where populations are particularly vulnerable. Awareness of these manifestations and adaptation strategy are key concerns for the continent for the coming years, especially in many domains such as agriculture, water, soils, and vegetation.

Coastal region and in particular low-lying estuary system have retained our attention for this study due to the fact that these low gradient areas would be the most affected areas as they represent the environmentally most sensitive areas.

As defined by Pritchard (1967), according to settings and mixing process (the type of river water and seawater mixing and the degree of salinization), estuaries may be subdivided into two groups. The first group includes normal estuaries, in which freshwater dilutes seawater and water salinity monotonically decreases downstream the river from 10–40 to 0.5–1 ‰ and the water runoff and precipitation exceed evaporation losses. The second group includes reverse, or hypersaline, estuaries, in which the salinity of estuarine water substantially exceeds the salinity of seawater; water evaporation losses exceed freshwater river runoff and precipitation. The first group is widespread in the world, and processes occurring are relatively well understood (Pritchard 1967; Ketchum 1983; McDowell and O'Connor 1983). The processes of mixing of river water and seawater in such estuaries are usually subdivided into three types: (1) complete mixing through the depth and weak density stratification of waters; (2) partial (moderate) mixing and moderate

stratification of waters; and (3) a saltwater wedge and intense stratification of waters (Mikhailov and Isupova 2008). Reverse estuaries are less common in the world and are poorly studied, peculiarities of the processes in reverse estuaries, including the processes occurring in the basin of the Caspian Sea (the Kayak Bay) as well as in west Africa and Australia (Wolanski 1986; Pagès et al. 1987). Under extremely arid condition, particularly during the dry season and drought lasting for many years, considerable deficiency of freshwater may occur in the river mouth reach.

Estuaries systems in semiarid and arid regions are characterized by highly variable seasonal river discharge; they represent in fact the most vulnerable zones with regard to climate variability and climate change. In some regions, with the persistence of drought periods and their consequence of negative water budget (induced by high evaporation effects), seawater may intrude into these systems and salinity will rise monotonically to hypersalinity with distance from the mouth (Ridd and Stieglitz 2002). Such a process has occurred in a coastal river in Senegal, namely the Saloum, actually a tide-influenced inverse estuary. In the Saloum estuary, saltwater contamination constitutes a serious problem. Evaporation and tidal inundation cause salt concentrations in the groundwater to rise above the normal seawater value. Ridd and Sam (1996), Sam and Ridd (1998) found that water inundating the salt flats returns to the estuary with a greater salinity by dissolving salt crystals. The intermittent and reverse flows of the Saloum River due to the runoff deficit caused saltwater advance up to 60 km upstream, contaminating surface waters, groundwater, and large areas of agricultural soils located in these zones. Salinity in the Saloum River showed a gradual upstream increase from 36.7 ‰ at the mouth to more than 90 ‰ at Kaolack (Pagès and Citeau 1990).

In arid and semiarid regions, soils salinity and saltwater intrusion are one of the major threats to agriculture (Ghassemi et al. 1995). Under most global warming scenarios, rate of coastal erosion will accelerate in the twenty-first century (Zhang et al. 2004; IPCC 2007). Remote sensing techniques have potential for mapping and monitoring the degree and extent of salinization. Thus, quantifying and monitoring their spatial distribution are very important for management purposes. Change detection is the process of identifying differences in the state of an object or phenomenon by observing it at different times (Singh 1989). It is one of the major applications of remotely

sensed data obtained from Earth-orbiting satellites because of repetitive coverage at short intervals and consistent image quality (Anderson 1977; Ingram et al. 1981; Nelson 1983). Change detection using images has been traditionally performed by comparing the classification of multitemporal data sets or by image processing techniques such as differencing and rationing. Change detection is useful in such diverse applications as land-use change analysis, monitoring of shifting cultivation, assessment of deforestation, changes in vegetation phenology, seasonal changes in pasture production, damage assessment, crop stress detection, disaster monitoring snow-melt measurements, daylight analysis of thermal characteristics, and other environmental changes (Singh 1989).

In change detection processes (Singh 1989; Coppin and Bauer 1994; Lu et al. 2003, 2004a, b; Coppin et al. 2004; Pu et al. 2008; Pan et al. 2011; Datta and Deb 2012; Petropoulos et al. 2012), time series images acquired from different dates are compared to analyze the spectral difference, caused by land-use/land-cover change (LULC) over time while trying to normalize other conditions to similar levels during that period. Therefore, it is necessary to confirm the estuary dynamic for mapping and monitoring the land-cover change with different techniques. Satellite remote sensing has been widely applied and recognized as a powerful and effective tool for detecting land-use and land-cover changes. However, according to the change's indices adopted and the methods of detection applied, results obtained show significant differences that can be evaluated both quantitatively (importance of the changes over time) and qualitatively (types of changes observed). Works of Smits et al. (1999) and Coppin et al. (2004) identified ten types of detection methods that are based on different techniques of image processing, including image subtraction, crossing classifications, principal component analysis (PCA: statistical analysis multivariate), vector calculating change, or neural networks.

In this study, two change detection techniques are evaluated: a classification method and a normalized remote sensing technique—normal difference vegetation index (NDVI) differencing method, focusing on a comparison between the two techniques and also on the determination of the threshold of the NDVI differencing method. Both techniques are common and effective in change detection of LULC (Gong and Howarth 1992; Kontoes et al. 1993; Fody 2004; San Miguel-Ayanz and Biging 1997; Aplin et al. 1999; Stuckens et al. 2000; Franklin et al. 2002; Pal and Mather 2004; Gallego 2004; Lu et al. 2004a, b; Pu et al. 2008; Datta and Deb 2012). Classification and NDVI differencing change detection methods were adopted in this study to analyze land-cover changes associated with salinization.

Study Area

The Saloum estuary system, located approximately between longitudes 14°01' and 16°56' W and latitudes 13°31' and 14°57' N (Fig. 1), shrank after the last pluvial episode in around 10,000 BC and represents one of the largest African reverse estuaries. It consists of an extensive network of fossil, dried secondary channels (so-called thalwegs) stretching north and eastward. The terrain in the study area is generally flat with altitudes ranging from below sea level in the estuarine zone to about 40 m above mean sea level (a.m.s.l.) inland; the longitudinal slope of the river course is correspondingly low as well as the shallow bathymetry of the river. The climate is Sudano-Sahelian type with a long dry season from November to June and a 4-month rainy season from July to October. The regional annual precipitation, which is the main source of freshwater recharge to the superficial aquifer, increases southward from 600 to 1,000 mm. The average temperature is 28–29 °C, and the average annual evaporation varies from 1,500 to 2,500 mm (source: meteorological data). The geomorphology consists of a gently sloping plain that extends toward the coast, ranging in elevation from 0 m in the estuary system to 40 m a.m.s.l. inland (Barousseau et al. 1985; Diop 1986). Sand dune deposits occur near the coast with an altitude of 1 m in the northern part and between 2 and 8 m a.m.s.l. in the southern part of the region. The hydrologic system of the region is characterized by the river Saloum, its two tributaries (Bandalia and Diomboss), and numerous small streams locally called “bolons.” Downstream, it forms a large low-lying estuary bearing tidal wetlands, a mangrove ecosystem, and vast areas of denuded saline soils called “tan” locally.

Methodology

Landsat data were selected to generate time series of land-cover changes in Saloum estuary. The regular revisit times and spatial resolution of the Landsat mission are well suited for regional, national, and global land-use changes. Four images were selected for this study dated October 17, 1984, October 31, 1992, November 01, 1999, and November 26, 2010, respectively. Accordingly, the study period covered about the last three decades.

The methodology applied in this work consists of three major steps: (1) collect and clean training samples; (2) automatic classification for LULC (land-cover–land-cover) mapping; and (3) NDVI differencing analysis. The images were selected with respect to resolution, number of bands, and season. Although the four scenes were already georeferenced to the UTM Zone 28 North and WGS 84 projection, they were geomatching. The outputs of the second and

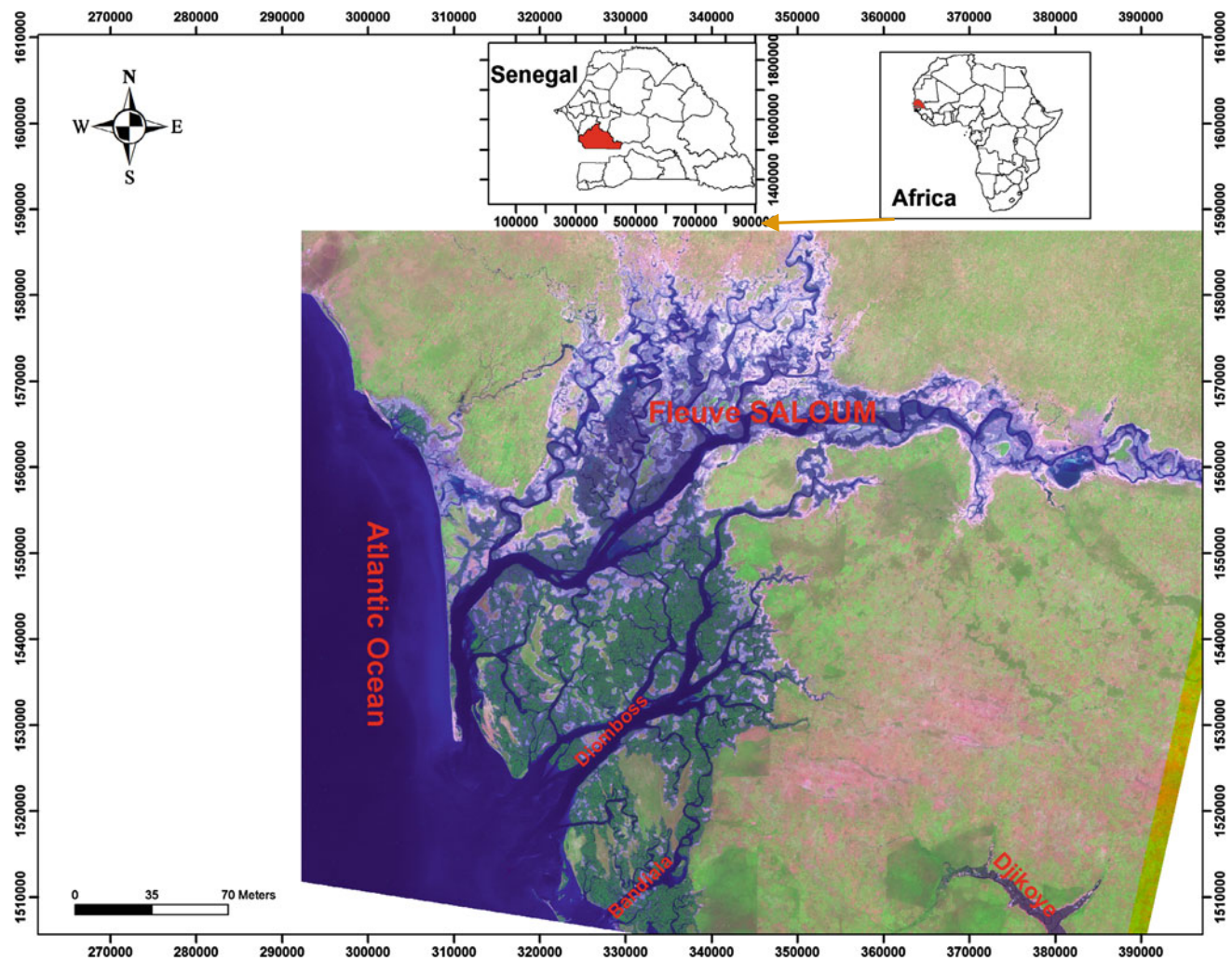


Fig. 1 A location map of the study site

third steps were combined to get the final conclusions. In this way, combination of the thematic information and the NDVI was possible in order to infer the nature of change, between-class or within-class change (Lunetta and Elvidge 1998), or simply an error.

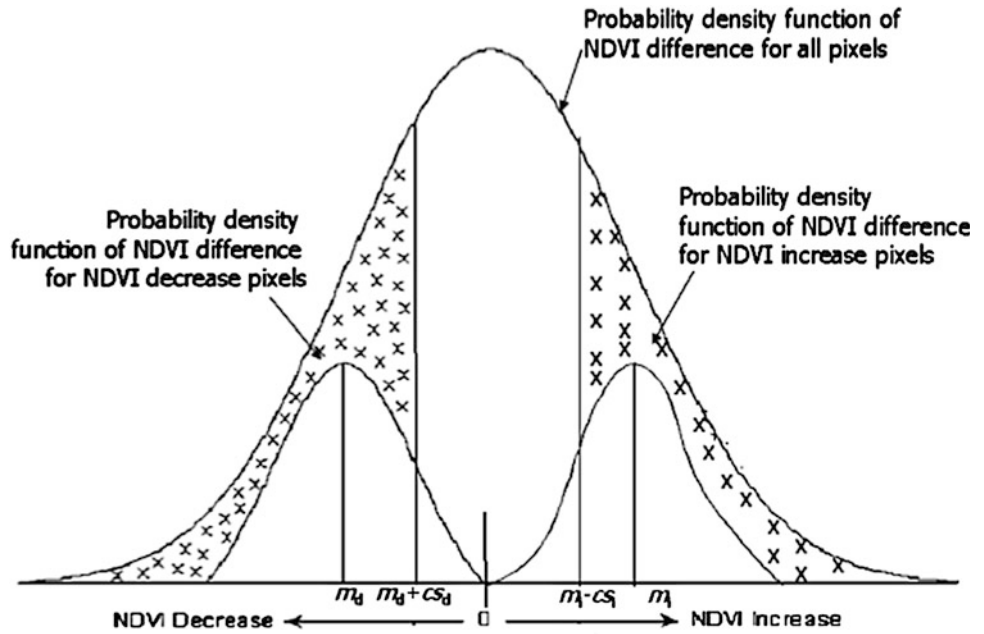
Detecting Outliers and Cleaning Training Sample

A suitable classification system and a sufficient number of training samples are prerequisites for a successful classification (Lu and Weng 2007). Training samples are usually collected from fieldwork or from fine spatial resolution aerial photographs and satellite images, and sampling of sufficient number and their representativeness is critical for image classifications (Landgrebe 2003; Mather 2004). Different collection strategies, such as single pixel, seed, and polygon, may be used, but selecting sufficient training

samples becomes difficult to perform when the landscape is complex and heterogeneous as they would influence classification results, especially for classifications with fine spatial resolution image data (Chen and Stow 2002). This problem would be complicated if medium or coarse spatial resolution data are used for classification, because a large volume of mixed pixels may occur (Lu and Weng 2007).

Despite precautions made in the training samples' collection, it is sometimes difficult to identify the most sensitive reference land-cover class for some observations, even resorting to ancillary data (Carrão et al. 2008). Thus, the original training sample, i.e., the sample of pixels that was directly collected by the analyst, contained unusual training units. According to Johnson and Wichern (1998), unusual observations are those that are either too large or too small compared to the others. Thus, in order to identify these anomalies, it is necessary to apply a statistical procedure based on the distance of each training unit to its mean class.

Fig. 2 Illustration of the two assumptions (adapted from Pu et al. 2008)



Let $\Omega = \{w_1, w_2, \dots, w_k\}$ be the set of class labels, μ_j the mean, and Σ_j the variance–covariance matrix of the j th class of Ω . Assuming that each land-cover class can be modeled by a multivariate normal distribution, it is possible to compute the squared Mahalanobis distance, for a given training unit t assigned to the j th class of Ω , by Eq. (1):

$$d_j^2(t) = (t - \mu_j)^T \Sigma_j^{-1} (t - \mu_j). \quad (1)$$

Under these assumptions, the d_j^2 is modeled by a chi-square random variable with k degrees of freedom, χ_k^2 , when the number of observations in each land-cover class is greater than 30 (Johnson and Wicher 1998). Thus, we can develop the following test to identify anomalous training units (Johnson and Wicher 1998). For every class w and for every training unit t of w , if $d_j^2(t)$ is greater than $\chi_k^2(\alpha)$, where α is the significance level of the test, we reject the hypothesis that t is a standard observation in class w ; otherwise, t is accepted and kept in the training sample. We have fixed the significance level at 2.5 %.

In practical applications, the class mean and variance–covariance matrix are not a priori known. Thus, we need to estimate them. To that end, we have estimated the class mean and variance–covariance using their standard maximum likelihood estimators, given by the following equations (Johnson and Wicher 1998):

$$\hat{\mu}_j = \frac{1}{n_j} \sum_{t \in w_j} t \quad (2)$$

$$\hat{\Sigma}_j = \frac{1}{n_j - 1} \sum_{t \in w_j} (t - \hat{\mu}_j)(t - \hat{\mu}_j)^T \quad (3)$$

where n_j is the number of training units in the j th class of Ω .

Supervised Image Classification

In recent years, many advanced classification approaches have been widely applied for image classification. Many factors, such as different sources of data, classification system, availability of classification software, and spatial resolution of the remotely sensed data, must be taken into account when selecting a classification method for use. Different classification methods have their own merits, and for the classification, we resort to the linear discriminant classifier (LDC). The LDC is a parametric classifier based on the homoskedasticity assumption, i.e., we assume that each land-cover class is modeled by a multivariate normal distribution and each of these distributions has an equal variance–covariance matrix. The LDC has many advantages over more sophisticated classification algorithms, due to the fact that it does not need as many training units comparing to the maximum likelihood classifier (MLC) or support vector machines (Hastie et al. 2009). It is simple in computational and operational terms and is reasonably robust (Kuncheva 2004), in that the results are good even when the classes do not have normal distributions.

Fig. 3 Classification result showing the land cover in Saloum estuary in October 1984 (a), October 1992 (b), November 1999 (c), and November 2010 (d)

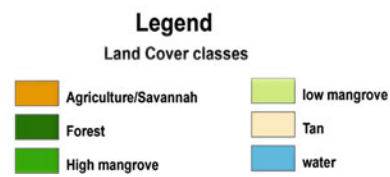
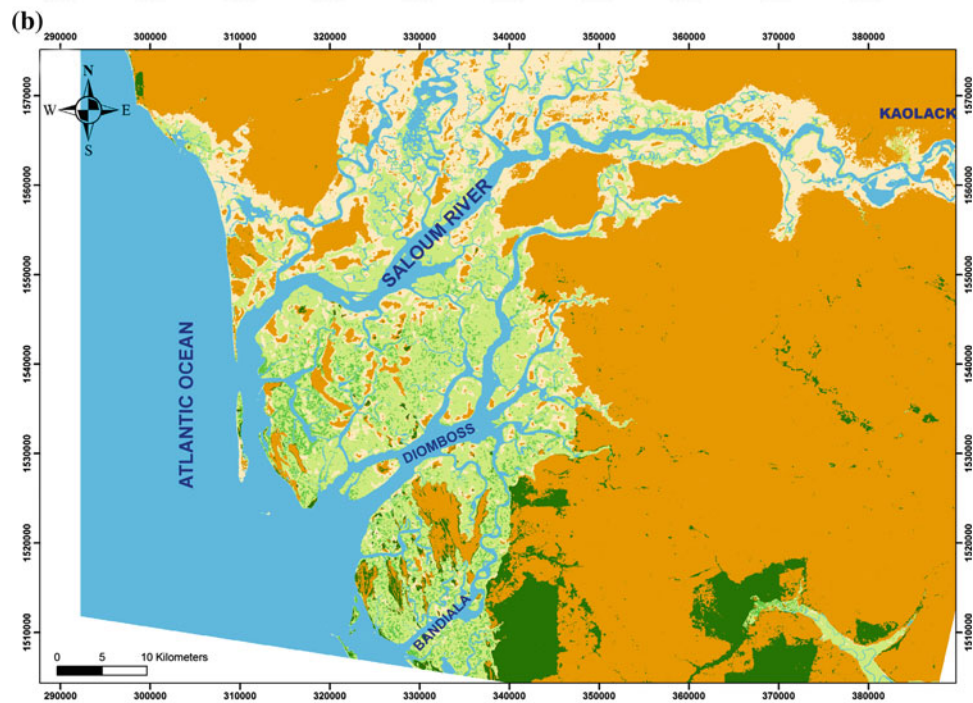
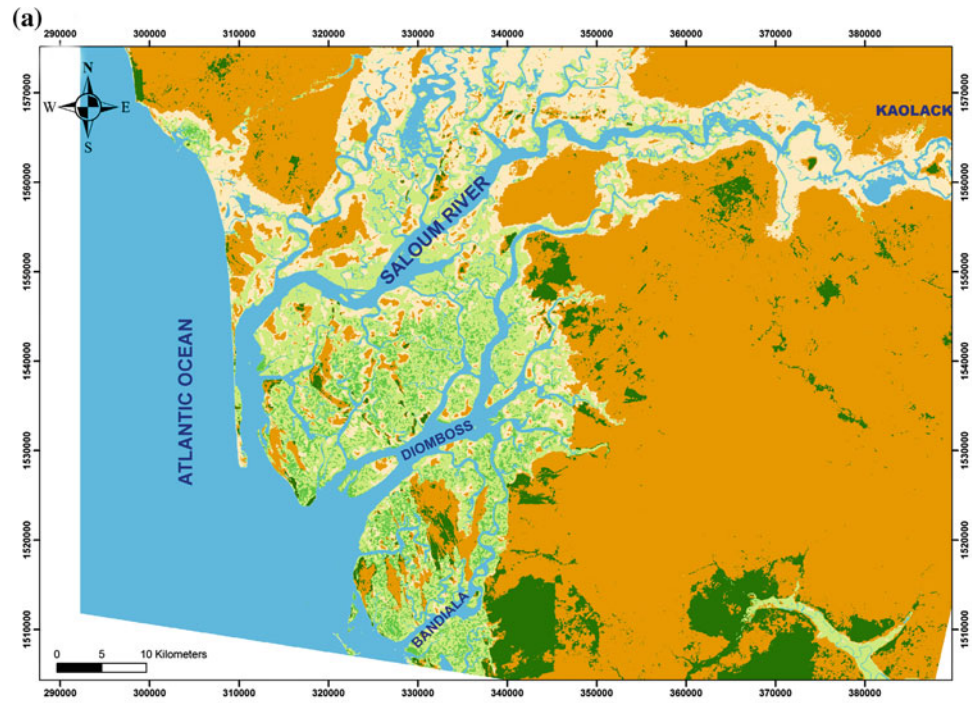


Fig. 3 continued

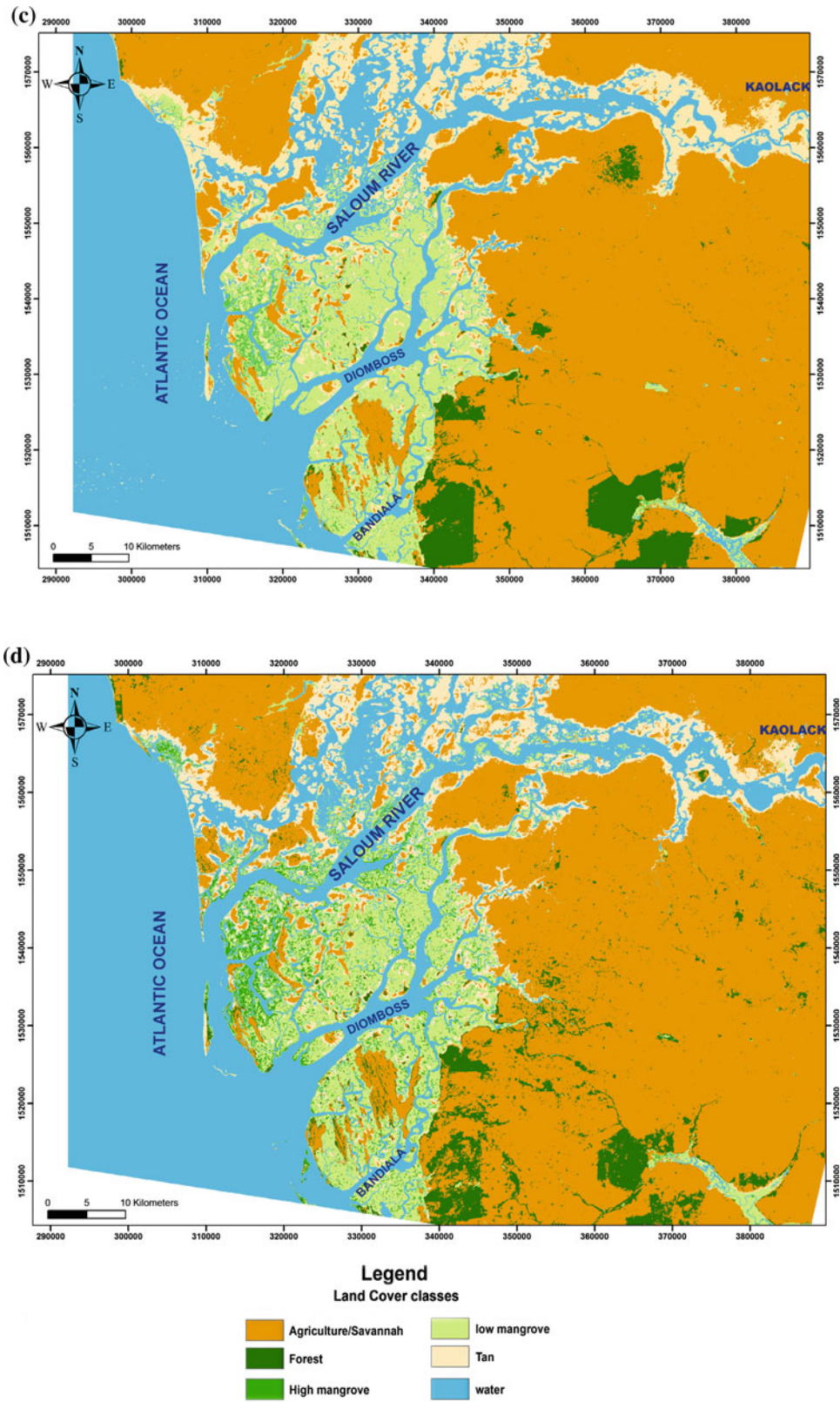


Table 1 Change matrices generated (%) through overlay analysis between the four single-date classification results, with the classification method

		Water	High mangrove	Low mangrove	“tan”	Savanna/rain-fed agriculture	Forest
		1992					
1984	Water	97	0	2	1	0	0
	High mangrove	2	42	55	0	0	0
	Low mangrove	5	4	83	6	1	1
	“tan”	1	0	7	83	9	0
	Savanna/rain-fed agriculture	0	0	0	1	98	1
	Forest	0	0	1	0	45	54
		1999					
1992	Water	96	0	2	2	0	0
	High mangrove	5	21	72	1	1	1
	Low mangrove	28	3	61	7	1	0
	“tan”	11	0	5	78	7	0
	Savanna/rain-fed agriculture	0	0	0	2	96	2
	Forest	0	0	2	1	26	70
		2010					
1999	Water	92	1	5	2	0	0
	High mangrove	10	44	43	1	1	1
	Low mangrove	12	14	66	4	3	1
	“tan”	18	0	7	63	12	1
	Savanna/rain-fed agriculture	0	0	0	1	95	3
	Forest	0	0	2	0	42	56

The bold represent the no change percentage.

From the pixel $x \in \mathbb{R}^k$ and the number of bands k , the label to be assigned to x is given by the class that maximizes the LDC discrimination function (Kuncheva 2004; Hastie et al. 2009). The LDC discrimination function is given, according to Kuncheva (2004), by Eq. (4):

$$h_i(x) = \frac{1}{2} \hat{\mu}_i^T \hat{\Sigma}^{-1} \hat{\mu}_i + \hat{\mu}_i^T \hat{\Sigma}^{-1} x \quad (4)$$

where $\hat{\Sigma}$ is the common variance–covariance matrix, estimated by the weighted average of the separately estimated class variance–covariance matrix, i.e.,

$$\hat{\Sigma} = \sum_{i=1}^k \frac{n_i}{n} \hat{\Sigma}_i \quad (5)$$

where n_i is the number of training units assigned to the i th class of Ω and n is the total number of training units.

The Landsat data of 1984, 1992, 1999, and 2010 are classified into six spectral classes using the LDC. Savanna and rain-fed agriculture are merged in the same class. This classification algorithm is a supervised parametric classifier, i.e., it requires a training sample in order to classify the pixel from a given image and it assumes that each land-cover class

behaves according to the normal statistic distribution. Thus, in this respect, it resembles the MLC. The difference is that the LDC is based on an additional assumption which is the homoskedasticity hypothesis, in which the classifier assumes that each class has equal variance, and thus, all covariance matrices are equal for every land-cover class of the nomenclature. Although the homoskedasticity hypothesis tends to be unrealistic, the literature has shown that this classifier behaves in a robust way even when there are deviations from the hypothesis of normality and homoskedasticity (Kuncheva 2004). The LDC has several advantages, in that it requires less training samples than the MLC and also it is easy to fine-tune and robust to noisy data (Hastie et al. 2009). In this sense, the LDC is a preferable classification algorithm for land-cover mapping (Carrão et al. 2008), especially when the image analyst does not have a reliable reference database to collect representative training samples. For the classification, a set of training sites and ground truth data were required. A sample set of 50 training sites was established. They characterize the six typical land-cover classes occurring in the study area. The sample plots were digitized on screen, and then, a supervised LDC was applied using a stack of the six (without band 6) original bands of the Landsat image and the remote sensing technique (NDVI) to generate a land-cover map.

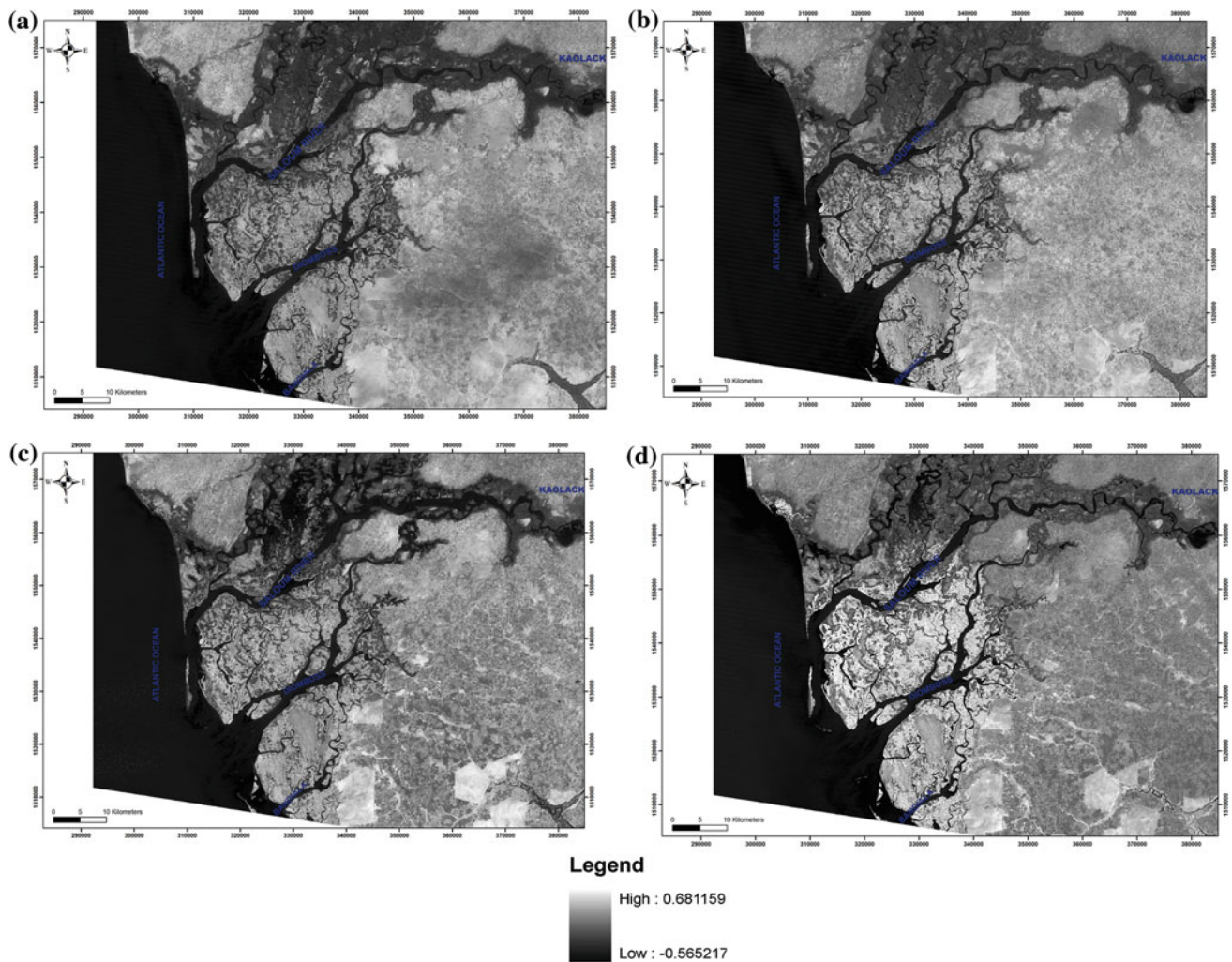


Fig. 4 NDVI images of the four Landsat images: **a** October 1984, **b** October 1992, **c** November 1999, and **d** November 2010. The NDVI images were calculated with the NIR band, the red band

The overall accuracy and a kappa analysis were used to perform a classification accuracy assessment based on error matrix analysis. Using the simple descriptive statistics technique, overall accuracy is calculated by dividing the total correct by the total number of pixels in the error matrix. The kappa analysis is a discrete multivariate technique used in accuracy assessments (Jensen 1996), and it yields a KHAT statistic (an estimate of kappa) which is a measure of agreement or accuracy (Congalton and Green 1993). It is a measure of overall statistical agreement of an error matrix, which takes non-diagonal elements into account, and it is recognized as a powerful method for analyzing a single error matrix and for comparing the differences between various error matrices (Congalton 1991; Smits et al. 1999; Foody 2004).

The next step was to generate a cross-tabulation using GIS technique that combines the information of two types of raster files into a contingency matrix. The procedure consists of counting pairs of categorical values of two given

variables in order to produce a categorical frequency distribution.

NDVI Differencing Method

The NDVI differencing method employs NDVI to differentiate images for mapping pixel change in the land-cover types. It is a popular vegetation index differencing used for change detection. For the NDVI differencing method, the NDVI image for each year was first computed according to Tucker (1978) using the NIR and RED bands (Eq. 6):

$$NDVI = \frac{NIR - RED}{NIR + RED} \tag{6}$$

NDVI is derived from differences in reflectance of the red (pigment absorption) and near-infrared (scattering from cellular structure), with values ranging from -1 to $+1$. Negative values refer to an absence of vegetation, while

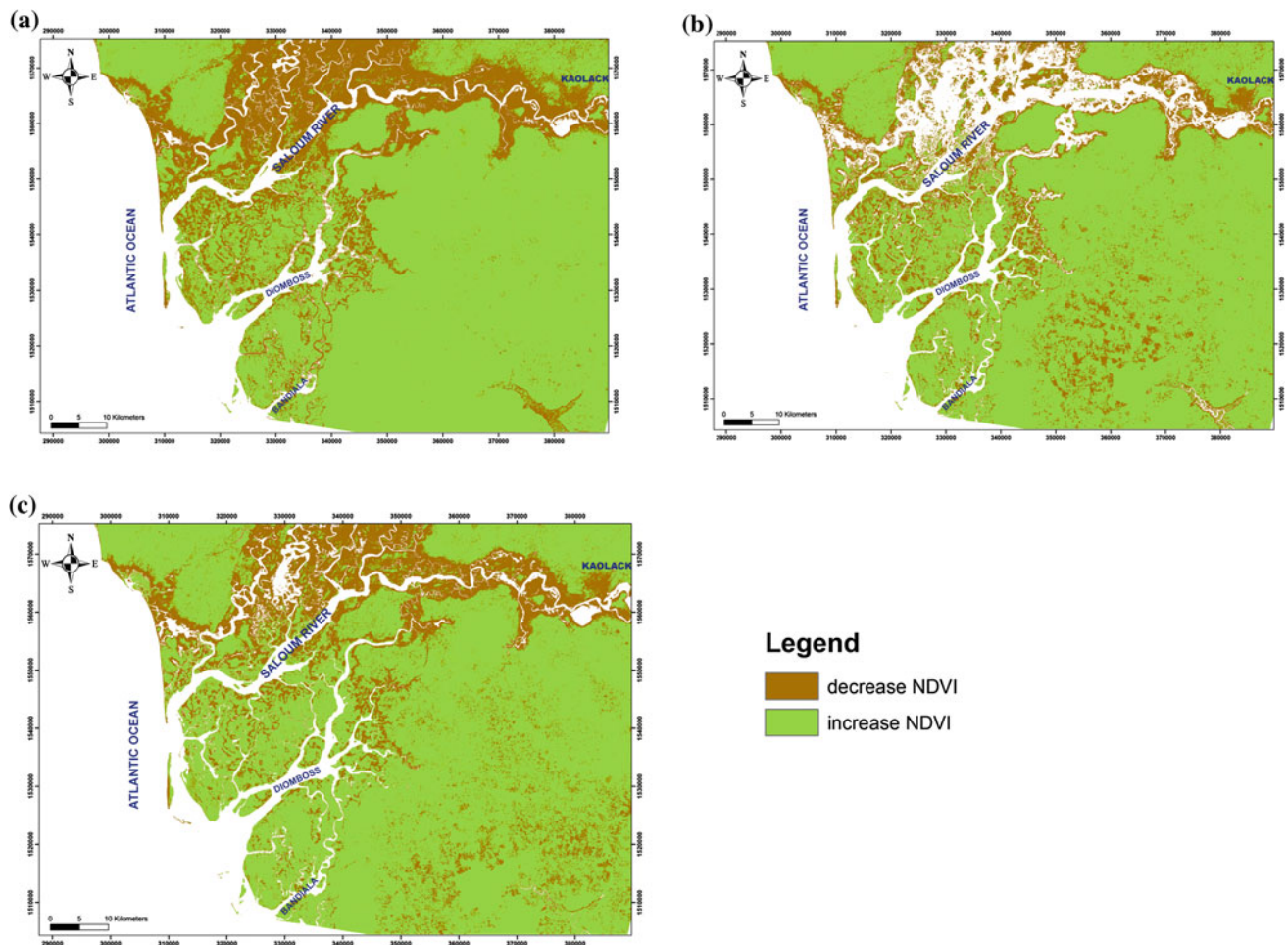


Fig. 5 Maps show areas of NDVI increase and areas of NDVI decrease between 1992 and 1984 (a), 1999 and 1992 (b), and 2010 and 1999 (c)

positive values are related to biomass variables, indicating leaf cover or productivity (Wang et al. 2003; Filella et al. 2004; Pettorelli et al. 2005; Zinnert et al. 2011).

Due to differences in atmospheric and land surface conditions and phenological stages, among other factors, during the acquisition, the satellite images exhibit differences in spectral behavior (Pu et al. 2008). The purpose of change detection is to extract the true LULC changes. Prior to that, it is important to normalize the images in order to identify the changes caused by other factors. It is worth noticing that the radiometric normalization does not completely correct the spectral behavior (Pu et al. 2008), i.e., the procedure will normalize the spectral values to a similar level for the two images acquired in different dates.

In this study, the normalization procedure was based on the work of Pu et al. (2008). The normalization was not done over the NIR and RED bands, but rather over the NDVI. This procedure required less time, due to the reduced number of samples necessary to collect when compared with normalizing the NIR and RED separately. In the normalization procedure, the NDVI values from one

date are assumed to be in a linear relation with the NDVI values from the other date. That is, it is possible to correlate using $y = ax + b$, where x is the pixel value of one image, y is its correspondent value, and a and b are coefficients determined by least-square linear regression (LSLR). The x image is usually called the reference image, and the y image is called the subject image (Lunetta and Elvidge 1998). To compute the LSLR parameters, it is necessary to collect a sample of pixel values. In this work, we have applied the pseudo-invariant feature (PIF) method described by Schott et al. (1988), to collect the samples. PIF are pixels that do not represent changes in their spectral response over the period of time in analysis. The PIF method is based on two poles, namely very dark pixels and very bright pixels. Typically, the dark PIFs can be found in deepwater pixels and the bright sets on surfaces with very little or no vegetation, like barren soil and rock (Lunetta and Elvidge 1998). These two poles are the basis to sample pixel values for normalization. Once the coefficients are determined, it becomes possible to apply the linear function to compute the predicted NDVI and then the difference between two

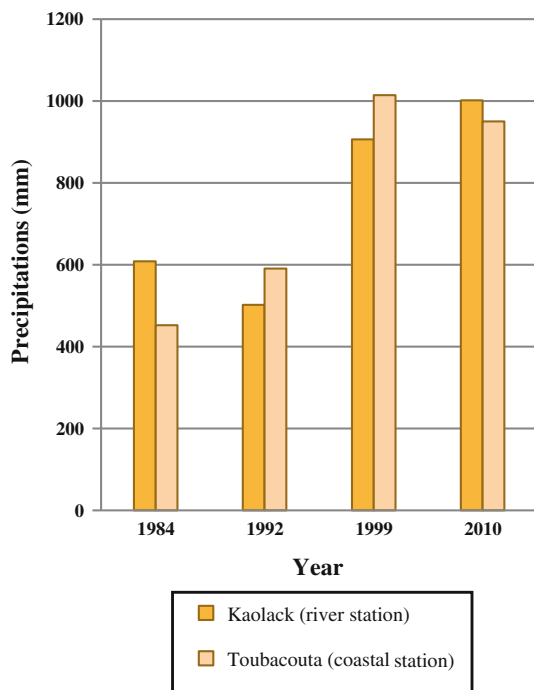


Fig. 6 Average mean annual precipitation (MAP) for 5 years prior to each date showing decreasing trend over time

dates, as suggested by Pu et al. (2008). In the present study, the NDVI differences between 1984 and 1992, 1992 and 1999, and 1999 and 2010 were computed.

After the computation of NDVI differences, the threshold values that will define the change/no-change areas must be computed. In this step, it is assumed that the difference in NDVI presents a normal distribution centered on zero (Lunetta and Elvidge 1998; Pu et al. 2008). In practice, this is usually not the case in that the NDVI differences have mean value very close but different to zero. Additionally, it is also assumed that NDVI increasing and decreasing parts present a normal distribution (Pu et al. 2008). Under these two assumptions, Pu et al. (2008) determined the threshold values that can be used to identify the change/no-change areas by computing the no-change interval: $[m_d + cs_d, m_i + cs_i]$, where m_d is the mean value and s_d is the standard deviation of the decreasing component; similarly for m_i, s_i (Fig. 2). The constant c can be determined using methods based on the kappa value or accuracy assessment (Pu et al. 2008). However, in this study, the NDVI differences presented a very small standard deviation value. This fact implies that the extreme values in the no-change interval tend to be very near to the global mean value. Thus, the threshold values were set as equal to the NDVI difference mean value. This raises the problem of how to detect no-change areas. To overcome this difficulty,

the LULC maps were used, so those pixels with equal thematic label were considered stable over time.

Under the two assumptions, the NDVI difference is centered on zero, and there is a value m_d , the mean value of the NDVI decreasing component, and a value m_i , the mean value of the NDVI increasing component. The no-change area is defined using the interval $[m_d + cs_d, m_i + cs_i]$.

Results and Discussions

Land-Cover Change

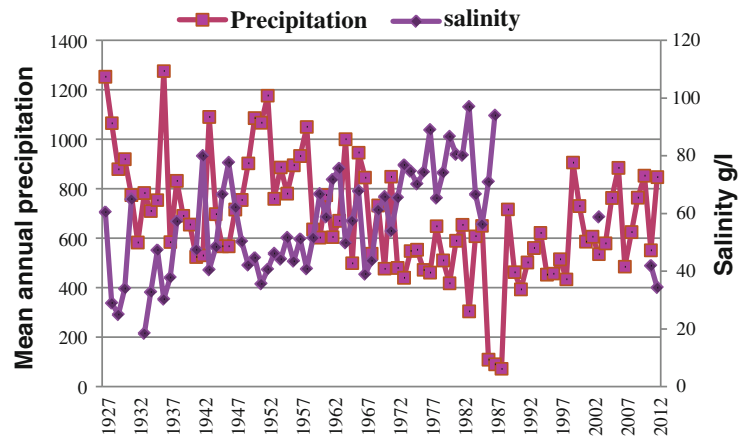
Classification

Using the classification method described above, the area of land-cover types in each of four study images was obtained and regional characterization of land-cover and land-cover changes was understood for Saloum estuary over the twenty-five-year period from 1984 to 2010. The results reveal that substantial changes took place during this time. The confusion matrices and kappa values were calculated from test samples for the four single-date classification results (Fig. 3): October 1984, October 1992, November 1999, and November 2010. The accuracy derived from the November 2010 image is evidently lower than that from 1984, 1992, and 1999 images (kappa value 0.79 vs. 0.90 or 0.87 or 0.85, or overall accuracy of 78 vs. 90 or 87 or 84 %). The lower classification accuracy might be due to the poorer quality of 2010 raw image strips in comparison with the other. Table 4 presents three change matrices that reflect the change directions and percentages of land-cover types based on the single-date classification results. The change matrices were calculated by overlaying the four single-date classification maps. The water area has increased in 1992 and 1999, and mangrove (high and low) and “tan” were lost by immersion because the break of the Sangomar spit in 1987. From 1984 to 1992, 55 % of high mangrove shifted to low mangrove and 6 % of low mangrove degraded to denudate soil (“tan”). These changes and conversions increased from 1992 to 1999, and 72 % of high mangrove transformed to low mangrove and 7 % of low mangrove and 3 % of savanna shifted to “tan” (Table 1). In 1999, due to high precipitation (Fig. 4) and sea level rise, the water surface also increased by 15 %.

NDVI Differencing

Over the NDVI images (Fig. 5), areas with gray reflect higher NDVI. From Fig. 4, the area reflecting higher NDVI (areas with gray) on the 2010 image is larger than that on the other three images. For NDVI index normalization between an NDVI image pair, the three linear regression equations are as follows:

Fig. 7 Interannual variation in salinity and rainfall at Kaolack locality from 1927 to 2012



$$y = 1.47x - 0.43 \quad (7)$$

$$R^2 = 0.98 \text{ for NDVI image pair } 1992 (y) - 1984 (x)$$

$$y = 0.73x + 0.29 \quad (8)$$

$$R^2 = 0.98 \text{ for NDVI image pair } 1999 (\cdot) - 1992 (x)$$

$$y = 1.7x + 0.02 \quad (9)$$

$$R^2 = 0.98 \text{ for NDVI image pair } 2010 (y) - 1999 (x)$$

For the NDVI image pairs 1992 (y) – 1984 (x) and 2010 (y) – 1999 (x), the slope coefficients, respectively, 1.4 and 1.7 reflect that the NDVI for the unchanged pixels increases. For the NDVI image pair 1999 (y) – 1992 (x), the NDVI for the unchanged pixels decreases due to precipitation increases in 1999, which is reflected in the 0.73 slope coefficient. These equations were used to predict the 1992 NDVI, the 1999 NDVI, and the 2010 NDVI images, respectively, from the 1984, 1992, and 1999 NDVI images. The three NDVI difference images were generated by subtracting the predicted NDVI from the actual NDVI.

In the period 1984–1992, 73.1 % of the study area showed an increasing NDVI, in 1992–1999 81 %, and in 1999–2010 79.5 %. Crossing these results with precipitation values for the same periods (Fig. 6), we can see that the increase in NDVI is caused by the increase in rainfall levels. Although the rainfall levels increased in those periods, the location of the areas that show decreasing NDVI is located in zones occupied by tan around the Saloum River due to the high salinity of the water river (Figs. 3 and 6). In fact, the land-cover maps show that the majority of the transitions that show NDVI are transition to decreasing tan.

Natural Factors of Estuary's Dynamic

Climate change has been particularly evident in west Africa in the last 30 years. Increased drought has led to a significant decrease in freshwater flow as well as an increase in the

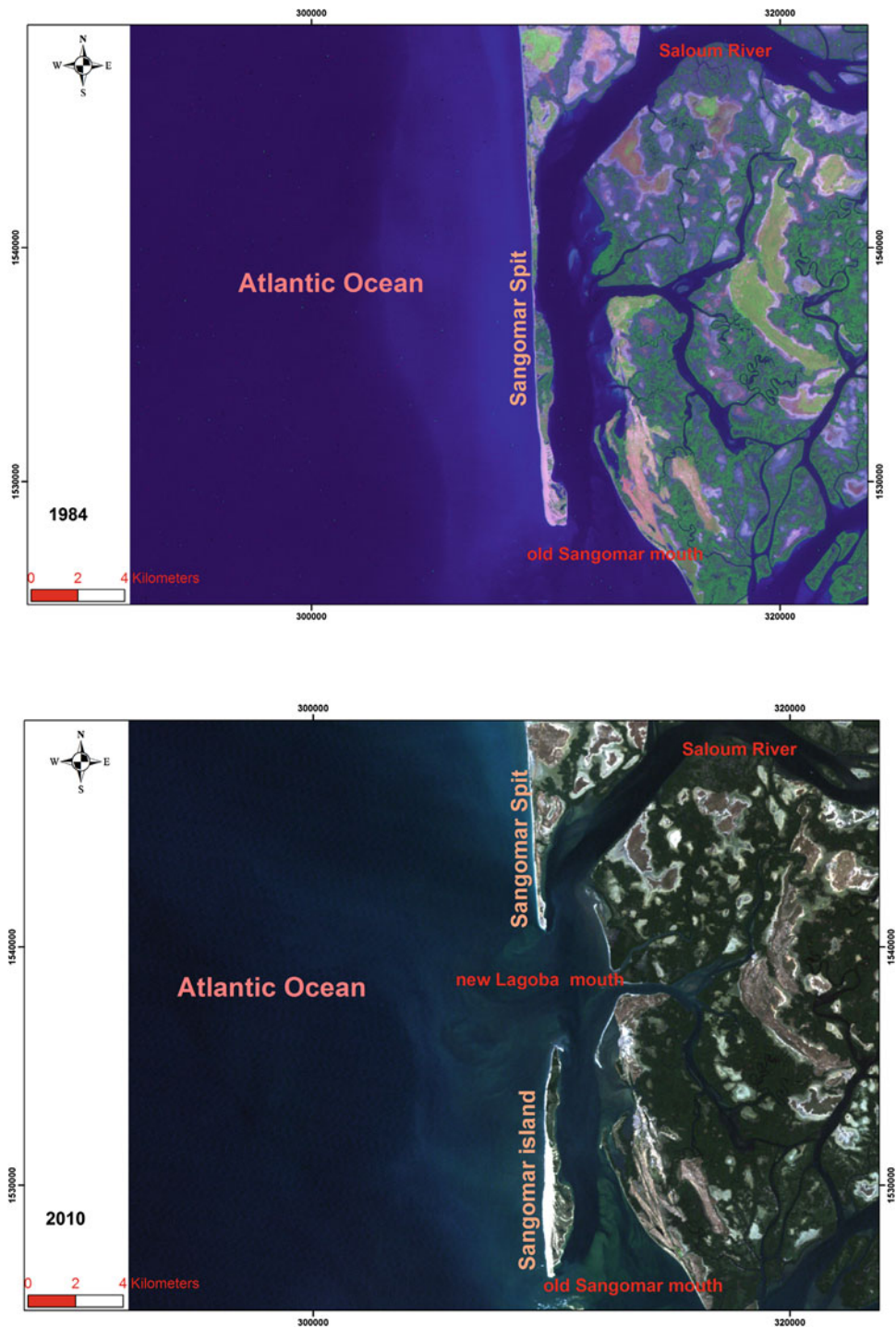
salinity level in estuary system. This is the case for the inverse estuary of the Sine Saloum where river waters with salinities much higher than seawater salinity occur (Fig. 7). In this region, the climate is characterized by an extended dry season, cool from November to March and warm from April to June, and by a short wet and warm season from July to October. Since the 1920s, the annual rainfall has decreased in this region with variable magnitude and drought period is much pronounced in recent decades (Pagès and Citeau 1990). The combined effects of reduced freshwater inputs, intense evaporation, and a low slope in the lower estuary have resulted in an overall high salinity and an inversion of the salinity gradient upstream the Saloum River course. This characteristic occurs to a lesser extent in the Diomboss branch.

The intermittent and the reverse flows of the Saloum River due to the runoff deficit caused saltwater advance up to 60 km upstream, contaminating surface water, groundwater, and large areas of agricultural soils located in these zones. Salinity in the Saloum River showed an upstream gradual increase from 36.7 ‰ at the mouth to higher than 90 ‰ at Kaolack (Pagès and Citeau 1990).

The chemical and isotopic data of water sampled in the Saloum River estuary (Faye et al. 2003, 2004, 2009; Dieng 2012 unpublished) revealed that high salinity is induced by seawater advance through tide dynamic. During the dry season (December to May) where maximum air temperatures and evaporation occur, seawater advance may reach 90 km inland (Kaolack locality) and salinity as high as 60 g/l (Dieng 2012 unpublished). Consequences of this high salinity are contamination of the shallow groundwater resources, large areas of arable land with formation of saline barren soils at the vicinity of the estuary system and the economically valuable mangrove ecosystem which plays a vital role to the majority of this rural population. The saltwater contamination constitutes a serious problem in this region.

Higher salinity content in the upstream estuary has also consequences on vegetation and soil resources in that the mudflat has been affected by these hydroclimatic variations. The morphopedological modifications induced by a high

Fig. 8 Evolution of the Sangomar sand spit between 1984 and 2010



salinization and acidification of soils have led to a gradual degradation, transformation, and disappearance of the mangrove to tan, and the most affected areas are located from the mid-to-upstream parts of the Saloum River (Figs. 3, 4 and 5). In addition to that, the Sangomar spit

break which occurred in 1987 (Diaw et al. 1991; Dieye et al. 2013) may contribute to the significant changes downstream (mangroves, land loss) since opening of the spit channel (4.96 km currently) favored direct hydraulic connection between the sea and the Saloum River (Fig. 8).

Conclusion

Uses of Landsat image allow us to monitor dynamic changes in land-cover and land-use over a large area. The image processing approach with GIS techniques can provide valuable spatial data for both quantitative and qualitative studies of the land-cover changes. This study showed that significant changes in land cover occur within the whole estuary system. These changes reflect environmental degradation, such as land desertification, salinization, and vegetation degradation, which are caused by salinity increase. Comparisons revealed that conversion of mangrove to “tan” cover was closely linked to precipitation and breaching of the Sangomar sand spit. In addition, these results show that significant changes in land cover occur in the study area, reflecting in this way environmental degradation and land desertification caused by the advance of salty bare lands.

Acknowledgements We thank ESA for providing us with Landsat imagery, TIGER capacity building, and IGP (Portuguese Geographic Institute) for giving us training job to enhance our knowledge in remote sensing and GIS.

References

- Anderson JR (1977) Land use and land cover changes. A framework for monitoring. *J Res Geol Surv* 5:143–153
- Aplin P, Atkinson PM, Curran PJ (1999) Per-field classification of land use using the forthcoming very fine spatial resolution satellite sensors: problems and potential solutions. In: Atkinson PM, Tate NJ (eds) *Advances in remote sensing and GIS analysis*. Wiley, New York, pp 219–239
- Barusseau JP, Diop EHS, Saos JL (1985) Evidence of dynamics reversal in tropical estuaries, geomorphological and sedimentological consequences (Saloum and Casamance Rivers, Senegal). *Sedimentology* 32(4):543–552
- Carrão H, Araújo A, Caetano M (2008) Land cover classification in Portugal with intra-annual time series of MERIS Images. In: *Proceedings of the 2nd MERIS/AATSR user workshop Frascati, Italy, 22–26 Sept 2008*
- Chen D, Stow DA (2002) The effect of training strategies on supervised classification at different spatial resolution. *Photogram Eng Remote Sens* 68:1155–1162
- Church JA, White NJ (2006) A 20th century acceleration in global sea-level rise. *Geophys Res Lett* 33:L01602
- Congalton RG (1991) A review of assessing the accuracy of classifications of remotely sensed data. *Remote Sens Environ* 37:35–46
- Congalton RG, Green K (1993) A practical look at the sources of confusion in error matrix generation. *Photogram Eng Remote Sens* 59:641–644
- Coppin PR, Bauer ME (1994) Processing of multitemporal landsat TM imagery to optimize extraction of forest cover change features. *IEEE Trans Geosci Remote Sens* 32:918–927
- Coppin PI, Jonckheere K, Nackaerts BM, Lambin E (2004) Digital change detection methods in ecosystem monitoring; a review. *Int J Remote Sens* 25:1565–1596
- Datta D, Deb S (2012) Analysis of coastal land use/land cover changes in the Indian Sunderbans using remotely sensed data. *Geo-spat Inf Sci* 15(4):241–250
- Diaw AT, Diop N, Thiam MD, Thomas YF (1991) Remote sensing of spit development: a case study of Sangomar sand spit, Senegal. *Z Geomorph Berlin-Stuttg* 81:115–124
- Dieye EHB, Diaw AT, Sané T, Ndour N (2013) Dynamique de la mangrove de l'estuaire du Saloum (Sénégal) entre 1972 et 2010. *Eur J Geogr*. <http://cybergegeo.revues.org/25671>; doi: 10.4000/cybergegeo.25671
- Diop ES (1986) Estuaires holocènes tropicaux. Etude géographique physique comparée des rivières du Sud du Saloum (Sénégal) à la Mellcorée (République de Guinée). Thèse Doctorat es Lettres Université L Pasteur Strasbourg. Tome I, p 522
- Faye S, Cissé Faye S, Ndoye S, Faye A (2003) Hydrogeochemistry of the Saloum (Senegal) superficial coastal aquifer. *Environ Geol* 44:127–136
- Faye S, Maloszewski P, Stichler W, Trimborn P, Cissé Faye S, Gaye CB (2004) Groundwater salinization in the Saloum (Senegal) delta aquifer: minor elements and isotopic indicators. *Sci Total Environ* J Springer. doi:10.1016/j.scitotenv.2004.10.00,17p
- Faye S, Diaw M, Ndoye S, Malou R, Faye A (2009) Impacts of climate change on groundwater recharge and salinization of groundwater resources in Senegal. In: *Groundwater and climate in Africa proceeding of the Kampala conference*. IAHS Publ 334, June 2008
- Filella I, Penuelas J, Llorens L, Estiarte M (2004) Reflectance assessment of seasonal and annual changes in biomass and CO₂ uptake of a Mediterranean Shrubland submitted to experimental warming and drought. *Remote Sens Environ* 90(3):308–318
- Foody GM (2004) Thematic map comparison: evaluating the statistical significance of differences in classification accuracy. *Photogram Eng Remote Sens* 70:627–633
- Franklin SE, Peddle DR, Dechka JA, Stenhouse GB (2002) Evidential reasoning with Landsat TM, DEM and GIS data for land cover classification in support of grizzly bear habitat mapping. *Int J Remote Sens* 23:4633–4652
- Gallego FJ (2004) Remote sensing and land cover area estimation. *Int J Remote Sens* 25:3019–3047
- Ghassemi F, Jakeman AJ, Nix HA (1995) Salinization of land and water resources. Human causes, extent, management and case studies. Sydney University of New South Wales Press Ltd.
- Gong P, Howarth PJ (1992) Frequency-based contextual classification and gray-level vector reduction for land-use identification. *Photogram Eng Remote Sens* 58:423–437
- Hastie T, Tibshirani R, Friedman J (2009) *The elements of statistical learning: data mining, and prediction*. Springer series in statistics, Springer. ISBN-10 0387848570
- Ingram K, Knapp E, Robinson JW (1981) Change detection technique development for improved urbanized area delineation. Technical memorandum CSC/TM-81/6087. Silver Spring, Computer Science Corporation, MD, USA
- IPCC (2007) *The physical science basis*. In: Solomon S et al (eds) *Contribution of working group I to the fourth assessment report of the intergovernmental panel on climate change*. Cambridge University Press, New York, pp 747–845
- Jensen J R (1996) *Introductory digital image processing*. Prentice Hall, New Jersey, USA
- Johnson RA, Wichern DW (1998) *Applied multivariate statistical analysis*. Prentice Hall, pp 816
- Ketchum BH (1983) *Estuarine characteristics, estuaries and enclosed seas*. Elsevier Science Publication Comp, Amsterdam, pp 1–14
- Kontoes C, Wilkinson G, Burrill A, Goffredo S, Megier J (1993) An experimental system for the integration of GIS data in knowledge-based image analysis for remote sensing of agriculture. *Int J Geogr Inf Syst* 7:247–262
- Kuncheva L (2004) *Combining pattern classifiers methods algorithms*, 1st edn. Wiley-Interscience. ISBN-10: 0471210788
- Landgrebe DA (2003) *Signal theory methods in multispectral remote sensing*. Wiley, Hoboken

- Lu D, Weng (2007) A survey of image classification methods and techniques for improving classification performance. *Int J Remote Sens* 28(5):823–870
- Lu D, Mausel P, Brondizio E, Moran E (2003) Change detection techniques. *Int J Remote Sens* 25:2365–2407
- Lu D, Mausel P, Batistella M, Moran E (2004a) Comparison of land-cover classification methods in the Brazilian Amazon Basin. *Photogram Eng Remote Sens* 70:723–731
- Lu D, Valladares G, Li GS, Batistella M (2004b) Mapping soil erosion risk in Rondonia, Brazilian Amazonia: using RUSLE, remote sensing and GIS. *Land Degrad Dev* 15:499–512. doi:[10.1002/ldr.634](https://doi.org/10.1002/ldr.634)
- Lunetta R, Elvidge C (1998) Remote sensing change detection: environmental monitoring and application. Taylor and Francis, Sleeping Bear Press, Inc.
- Mather PM (2004) Computer processing of remotely-sensed images: an introduction, 3rd edn. Wiley, Chichester
- McDowell DM, O'Connor BA (1983) Гидравлика приливныkh уст'ev rek (hydraulics behaviour of estuaries). Energoatomizdat, Moscow
- Mikhailov VN, Isupova MV (2008) Hypersalinization of river estuaries in West Africa. *Water Resour* 35(4):367–385
- Nelson RF (1983) Detecting forest canopy change due to insect activity using landsat MSS. *Photogram Eng Remote Sens* 49:1303–1314
- Overpeck JT, Otto-Bliesner B, Miller GH, Mush DR, Alley RB, Kiehl JT (2006) Paleoclimatic evidence for future ice-sheet instability and rapid sea-level rise. *Science* 311(5758):1747–1750. doi:[10.1126/science.1115159](https://doi.org/10.1126/science.1115159)
- Pagès J, Citeau J (1990) Rainfall and salinity of a Sahelian estuary between 1927 and 1987. *Hydrol J* 113(1–4):325–341
- Pagès J, Debenay JP, Lebrusq JI (1987) L'environnement estuarien de la Casamance. *Rev Hydrobiol Trop* 20(3–4):191–202
- Pal M, Mather PM (2004) Assessment of the effectiveness of support vector machines for hyperspectral data. *Future Gener Comput Syst* 20:1215–1225
- Pan W, Xu H, Chen H, Zhang C, Chen J (2011) Dynamics of land cover and land use change in Quanzhou city of SE China from landsat observations. *Electr Eng* 40371107:1019–1027
- Petropoulos G, Partsinevelos P, Mitraka Z (2012) Change detection of surface mining activity and reclamation based on a machine learning approach of multitemporal landsat TM imagery. *Geocarto Int*. doi:[10.1080/10106049.2012.706648](https://doi.org/10.1080/10106049.2012.706648)
- Pettorelli N, Vik JO, Mysterud A, Gaillard JM, Tucker CJ, Stenseth NC (2005) Using the satellite-derived NDVI to assess ecological responses to environmental change. *Trends Ecol Evol* 20(9):503–510
- Pritchard DW (1967) What is an estuary: physical viewpoint, estuaries. American Association Advanced Science Publication, Washington, DC
- Pu R, Gong P, Tian Y, Miao X, Raymond IR, Carruthers GL, Anderson GL (2008) Using classification and NDVI differencing methods for monitoring sparse vegetation coverage: a case study of saltcedar in Nevada, USA. *Int J Remote Sens* 29(14):3987–4011
- Ridd PV, Sam R (1996) Profiling groundwater salt concentration in mangrove swamps and tropical salt flats. *Estuar Coast Shelf Sci* 43:627–635
- Ridd PV, Stieglitz T (2002) Dry season salinity changes in arid estuaries fringed by mangroves and saltflats. *Estuar Coast Shelf Sci* 54:1039–1049
- Sam R, Ridd PV (1998) Spatial variations of groundwater salinity in a mangrove salt flat System Cocoa Creeks Australia. *Mangroves Salt Marshes* 2:121–132
- San Miguel-Ayanz J, Biging GS (1997) Comparison of single-stage and multi-stage classification approaches for cover type mapping with TM and SPOT data. *Remote Sens Environ* 59:92–104
- Singh A (1989) Digital change detection techniques using remotely-sensed data. *Int J Remote Sens* 10:989–1003
- Smits PC, Dellepiane SG, Schowengerdt RA (1999) Quality assessment of image classification algorithms for land-cover mapping: a review and a proposal for a cost-based approach. *Int J Remote Sens* 20(8):1461–1486
- Stuckens J, Coppin PR, Bauer ME (2000) Integrating contextual information with per-pixel classification for improved land cover classification. *Remote Sens Environ* 71:282–296
- Tucker CJ (1978) A comparison of satellite sensor bands for vegetation monitoring. *Photogram Eng Remote Sens* 44(11):1369–1380
- Wang J, Rich PM, Price KP (2003) Temporal responses of NDVI to precipitation and temperature in the central great plains, USA. *Int J Remote Sens* 24(11):2345–2364
- Wolanski E (1986) An evaporation-driven salinity maximum zone in Australian tropical estuaries. *Estuar Coast Shelf Sci* 22:415–424
- Zhang K, Douglas BC, Leatherman SP (2004) Global warming and coastal erosion. *Clim Change* 64(1–2):41–58
- Zinnert JC, Shifflett SA, Vick JK, Young DR (2011) Woody vegetative cover dynamics in response to recent climate change on an Atlantic coast barrier island: a remote sensing approach. *Geocarto Int* 26(8):595–612